4th Intercontinental Geoinformation Days

igd.mersin.edu.tr

Analysis of heat island formation in land use of Ardabil city using thermal remote sensing imagers

Hossein Fekrat*[1], Sayyad Asghari Saraskanrood [1], Seyed Kazem Alavipanah [2]

[1] *University of Mohaghegh Ardabili, Faculty of Social Sciences, Department of Natural Geography, Ardabil, Iran*
[2] *University of Tehran, Faculty of Geography, Department of Remote Sensing and GIS, Tehran, Iran*

Keywords
LST
Application
Single channel
GEE
Moran global indices

Abstract

Land surface temperature (LST) is one of the essential parameters of environmental science studies. In this study the land surface temperature of Ardabil city using a LST automatic calculator application was estimated with a single channel algorithm. for this purpose, Landsat 5 and 8 satellite images on 2000/07/31 and 2019/08/21 were used. In order to validate the LST map of the application output in addition to the data of two meteorological stations in the study area, from the surface temperature of two ground stations that were recorded simultaneously with the satellite was also used. Finally using the LST map, hot spots analysis and hot and cold clusters of thermal islands of Ardabil city were extracted. Also, using the GEE web platform, the land use map of the study area with the RF algorithm was prepared. The analysis spatial correlation with Moran global indices showed the land surface temperature of Ardabil city has a spatial structure and are distributed in clusters. The results showed that the lowest surface temperatures to water areas, irrigated agriculture and residential areas are formed and thermal cores are mostly created outside residential areas in barren lands rainfed agriculture and rangeland.

1. Introduction

Land surface temperature is an important indicator for studying environmental changes and the energy balance of the earth Which can be used to monitor the temperature changes of cities (Stephens and L'Ecuyer 2015). Urban areas continue to expand in population and built-up extent, with faster rates in developing countries (Nyamekye et al, 2020). its adverse impacts that include increased air pollution, surface urban heat islands and dust, significantly influence urban micro- and macro-climate and affect urban environmental quality and human health (Heaviside et al, 2016).

Remote sensing technology using satellite imagery can be a great help for managers and urban planners to study temperature conditions and land use changes in the past, evaluate current trends and ultimately predict and manage the future. For instance, missions such as Landsat offer large archival data spanning as far back as 1972 at reasonable and improved radiometric, spectral and spatial resolution, valuable for assessing both large scale and localized temporal and multi-temporal landscape and environmental patterns (Keramitsoglou at el, 2019). Recently, several studies around the world have been conducted on the formation of thermal islands and its effects on the urban environment. like the (Heaviside et al, 2016; Dutta et al, 2020; Zhao et al, 2021; Lee et al, 2021; You et al, 2021).

In this study, an application was designed to automatically calculate the land surface temperature. Due to the large area of the study and the insufficient number of meteorological stations and in order to synchronize the validation data with the satellite transit time, In addition to surface temperature data measured at synoptic stations, land surface temperature was recorded at two ground stations at the same time as the satellite.

* **Corresponding Author**

*(Hosseinf7181@gmail.com) ORCID ID 0000-0003-4306-1236
(asghari@uma.ac.ir) ORCID ID 0000-0002-5015-904X
(salavipa@ut.ac.ir) ORCID ID 0000-0002-3554-111X

Cite this study

Fekrat, H., Saraskanrood, S. A., & Alavipanah, S. K. (2022). Analysis of heat island formation in land use of Ardabil city using thermal remote sensing imagers. 4th Intercontinental Geoinformation Days (IGD), 114-117, Tabriz, Iran

2. Method

2.1. Study area

Ardabil city is located in the geographical range of 37 degrees and 55 minutes and 60 seconds to 38 degrees and 36 minutes and 27 seconds north latitude and 48 degrees and 39 minutes and 20 seconds to 47 degrees and 48 minutes and 21 seconds east longitude (Figure 1).

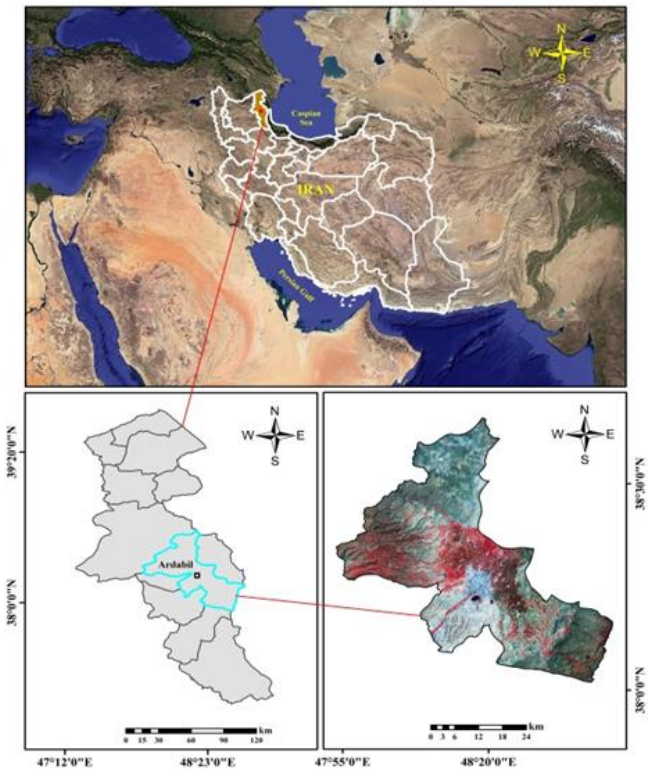

Figure 1. Location of the study area

2.2. Methodology

2.2.1. LST (Single Channel Algorithm)

Only first letter of first word is capital, left aligned, 10 font size, bold. It should be separated from the former paragraph with single line.

The generalized Single Channel Algorithm was developed was developed for the purpose of extracting LST from a single thermal infrared band (Jiménez-Muñoz and Sobrino 2003). According to the algorithm, the LST is expressed as shown in Equations (1–8).

$$LST = \gamma[\varepsilon^{-1}(\psi_1 L_{sensor} + \psi_2) + \psi_3] \quad (1)$$

$$\gamma = \left\{\frac{c_2 L_{sensor.\lambda}}{T^2_{sensor}}\left[\frac{\lambda^4}{c_1} L_{sensor\lambda} + \lambda^{-1}\right]\right\}^{-1} \quad (2)$$

$$C1 = 1.19104 \times 10^8 (W \cdot \mu m \cdot m^{-2} \cdot sr^{-1}) \quad (3)$$

$$C2 = 1.43877 \times 10^4 (\mu m4 \cdot K) \quad (4)$$

$$\delta = -\gamma L_{sensor.\lambda} + T_{sensor} \quad (5)$$

$$\psi_{1(\omega.T_a)} \equiv \frac{1}{\tau_{(\omega.T_a)'}} \quad (6)$$

$$\psi_{2(\omega.T_a)} \equiv -L^{\downarrow}_{atm(\omega.T_a)} - \frac{L^{\uparrow}_{atm(\omega.T_a)}}{\tau_{(\omega.T_a)'}} \quad (7)$$

$$\psi_{3(\omega.T_a)} \equiv -L^{\downarrow}_{atm(\omega.T_a)} \quad (8)$$

where ε and L_{senso} represent emissivity and thermal radiance, the γ gamma calculated using Equation 2, C1 and C2 Planck constant radiation coefficients, is δ equal to the delta obtained from equation 5, $L_{sensor\lambda}$ and T_{sensor} are equal to the radius of the thermal sensor, respectively (10 band TIRS sensor and 6 band TM sensor and ψ_1, ψ_2 and ψ_3 are atmospheric correction parameters.

2.2.2. Spatial Analysis of the LST

The geospatial dependence phenomenon is known as spatial autocorrelation, having a significant effect on the spatial distribution pattern of LST and the inherent driving forces utilizing statistical analysis. The global spatial autocorrelation analysis of this study is mainly based on Moran's I, reveals the aggregation of LST spatial layout as a whole, and indicates whether LST has spatial autocorrelation as follows (equation 9,10 and 11):

$$I = \frac{n \sum_{i=1}^{n} \sum_{i=1}^{n} w\,ij_{ZiZJ}}{S0 \sum_{i=1}^{n} zi^2} \quad (9)$$

$$S0 = \sum_{i=1}^{n}\sum_{i=1}^{n} w\,ij \quad (10)$$

$$Zi = \frac{i - E(I)}{\sqrt{V(I)}} \quad (11)$$

In general, if the value of the Moran index is close to +1 data have spatial autocorrelation and have a cluster pattern and if the value of the Moran index is close to -1, then the data are fragmented (Goodchild 1986).

GetisOrd G_i* (hot-pot analysis) reveals the significant high-value and low-value clusters in the spatial region and identifies the spatial distribution of LST cold and hot-spots in the region. Its formula is (Getis and Ord, 1992):

$$G_i = \frac{\sum_{j=1}^{n} W_{ij}X_j - X\sum_{j=1}^{n} W_{ij}}{S\sqrt{\frac{\left[n\sum_{j=1}^{n} W_{ij}^2 - \left(\sum_{j=1}^{n} W_{ij}\right)^2\right]}{n-1}}} \quad (12)$$

where G_i statistic is a z-score. The higher the z-score, the tighter the clustering of hot-spots (high values). The lower the z-score, the tighter the clustering of cold-spots (low values). Here, X_i and X_j are the LST at the location of grid i and j. $W_{i,j}$ is the spatial weight matrix, and X is the mean of LST.

3. Results and Discussion

Figure 2 shows the land surface temperature output maps using the 6-band TM sensor images and the 10-band TIRS band of Landsat 5 and 8 satellites for 2000/07/31 and 2019/08/21. In order to validate the accuracy of the output LST map of 2000, the surface temperature data of two meteorological stations were used and for the LST map of 2019, the surface temperature data of two meteorological stations and two ground stations were used and the result is shown in Table 1.

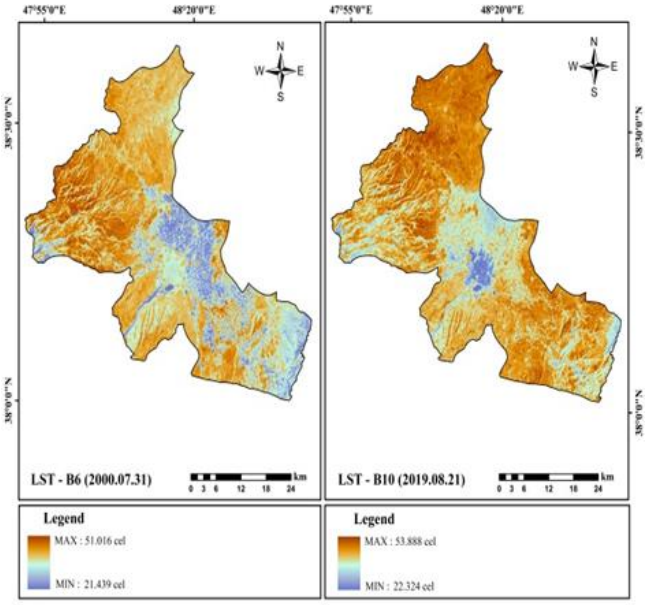

Figure 2. LST maps in 2000 and 2019

Table 1. Estimated LST difference with meteorological and ground station data

LST map	Station-1	Station-2	Station-3	Station-4
2000	+2.5	-2		
2019	+1.3	+0.9	-1	-0.9

To calculate Moran's correlation analysis, first the standard score of Z and P-value were calculated, the results of which are presented in Table 2. In the next step, the significance of Moran global correlation analysis was examined. Moran's global zero hypothesis states that spatial clustering is by no means formed between values. Based on the results of Table 2 and Figure 3, for both years the null hypothesis is rejected and confirms the existence of a relationship and spatial structure in the temperature values of Ardabil city.

Getis-Ord-Gi statistics for 2000 and 2019 were used to determine areas with high and low value clusters and hot and cold spots and the results are presented in Figure 4.

Table 2. Output of Moran index

p-value	Variance	z-score	Expected index	Moran Index	date
0	0.000003	540.443	-0.000005	0.8684	2000
0	0.000003	540.289	-0.000005	0.8682	2019

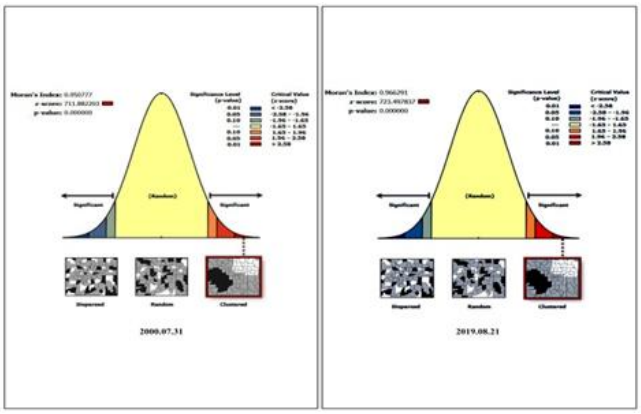

Figure 3. Graphic output of global Moran index for LST in Ardabil city

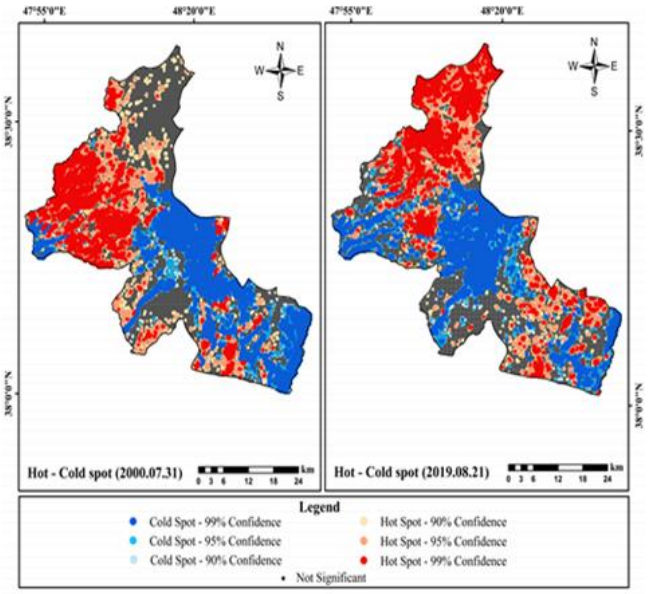

Figure 4. Hot and cold spots of Ardabil city

Figure 5 shows the land use map of Ardabil city, which has been prepared using the Random Forest algorithm in the gee platform with seven classes. to evaluate the trend of land surface temperature change, especially in the residential sector surface temperature profiles with a radius of 10 km are drawn around residential areas, the results of which are shown in Figure 5. The trend of the profiles shows that as the curve approaches the urban sector, the trend of the graphs gradually takes a downward shape. This trend of decreasing temperature in the urban sector reaches its lowest point and after passing this area, again due to rising temperatures, the upward trend.

4. Conclusion

The results of the study showed that the formation of thermal cores in 2000 was mainly in the northwestern parts and with a small amount in the northern and southern parts. while in 2019, the main thermal core of the city has been formed in the northern parts and with a lower percentage in the southeastern part, it seems that the main reason has been the disappearance of pastures in the northern parts in recent years. Also based on the values of Z and P and the value of the global Moran index, the land surface temperature in Ardabil city is

distributed in clusters and high and low temperature values tend to cluster. The results show the high temperature difference between the residential part of the region and other uses (agriculture, pastures and barren lands). Existence of agricultural lands with irrigated cultivation around the residential part is one of the main factors of low temperature in the central part of the region.

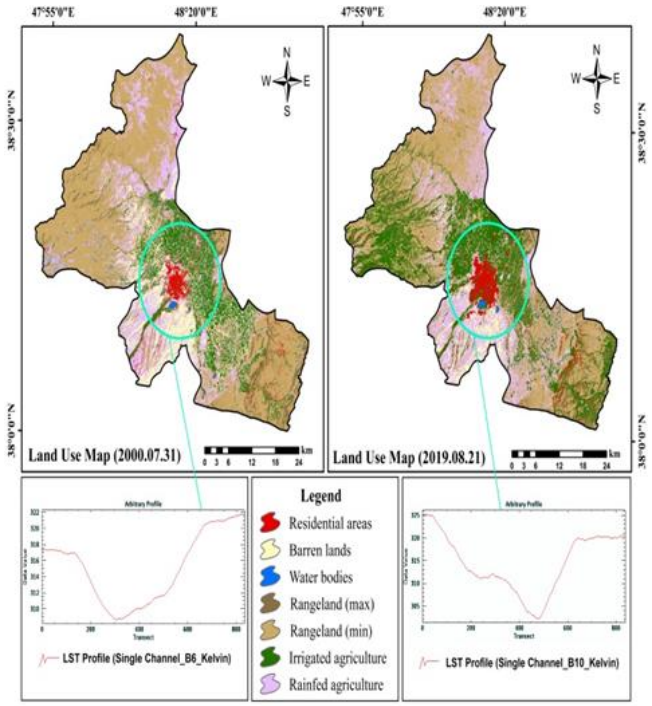

Figure 5. Land use map and surface temperature profile around the residential area with a radius of 10 km

References

Dutta, K., Basu, D., & Agrawal, S. (2021). Evaluation of seasonal variability in magnitude of urban heat islands using local climate zone classification and surface albedo. Int. J. Environ. Sci. Technol. 1–22.

Getis, A., & Ord, J. K. (1992). The analysis of spatial association by use of distance statistics. Geogr. Anal. 24, 189–206.

Goodchild (1986). spatial autocorrelation (CATMOG47). Geobooks, Norwich, UK.

Heaviside, C., Vardoulakis, S., & Cai, X. M. (2016). Attribution of mortality to the urban heat island during heatwaves in the West Midlands, UK. Environ. Health A Glob. Access Sci. Source, 15, 49–59.

Jiménez-Muñoz, J. C., & Sobrino, J. A. (2003). A generalized single-channel method for retrieving land surface temperature from remote sensing data. J. Geophys. Res. Atmos, 108.

Keramitsoglou, I., Kiranoudis, C. T., Ceriola, G., Weng, Q., & Rajasekar, U. (2011). Identification and analysis of urban surface temperature patterns in Greater Athens, Greece, using MODIS imagery. Remote Sens. Environ, 115, 3080–3090.

Lee, Y., Lee, S., Im, J., & Yoo, C. (2021). Analysis of Surface Urban Heat Island and Land Surface Temperature Using Deep Learning Based Local Climate Zone Classification: A Case Study of Suwon and Daegu, Korea. Korean J. Remote Sens. 37, 1447–1460.

Nyamekye, C., Kwofie, S., Ghansah, B., Agyapong, E., & Appiah, L. (2020). Land Use Policy Assessing urban growth in Ghana using machine learning and intensity analysis: A case study of the New Juaben Municipality. Land Use Policy, 99, 105057.

Stephens, G., L'Ecuyer, T. (2015). The Earth's energy balance. Atmos. Res, 166, 195–203. https://doi.org/10.1016/j.atmosres. 06.024.

You, M., Lai, R., Lin, J., & Zhu, Z. (2021). Quantitative Analysis of a Spatial Distribution and Driving Factors of the Urban Heat Island Effect: A Case Study of Fuzhou Central Area, China. Int. J. Environ. Res. Public Health, 18, 13088.

Zhao, C., Jensen, J. L. R., Weng, Q., & Currit, N. (2020). Use of Local Climate Zones to investigate surface urban heat islands in Texas Use of Local Climate Zones to investigate surface urban heat islands in Texas. GISci. Remote Sensing. 57, 1083–1101.